communications engineering

A Nature Portfolio journal

Article

https://doi.org/10.1038/s44172-025-00451-0

Ultrasonographic-guided robotic-assisted percutaneous nephrolithotomy

Stefano Bazzani[1] ✉, Stefano Puliatti[2], Stefania Ferretti[3], Giampaolo Bianchi[2], Cristian Secchi[1] & Federica Ferraguti[1]

Percutaneous nephrolithotomy (PCNL) is considered the gold standard for treating kidney stones larger than 20 mm. However, the procedure requires high expertise and technical skills, especially for precise and accurate percutaneous access. This paper presents a robotic system designed to enable accurate kidney access by combining 3D anatomical modeling with real-time ultrasound guidance, thereby allowing novice surgeons to gain confidence in performing the initial puncture. A comprehensive validation campaign was conducted in a controlled clinical simulation environment, with experiments performed by both experienced urologists and urology residents. The proposed system improves surgical performance, reduces human error, and makes the procedure more accessible to less experienced clinicians.

Percutaneous Nephrolithotomy (PCNL) is considered the gold standard for the treatment of patients with renal stones larger than 20 mm in diameter[1]. Its popularity and acceptance among urologists and patients is largely due to the fact that it is minimally invasive and is associated with low morbidity[2]. Using fluoroscopy and/or ultrasonographic (US) imaging the urologist inserts a hollow needle into one of the renal calyxes of the kidney, cadully avoiding adjacent organs and tissues. This pathway is then gradually dilated, and a percutaneous sheath is inserted to accommodate the nephroscope, which is the tool used to reach, fragment, and extract the stone.

Despite the global prevalence of kidney stones, which affects approximately 7–13% of the population in North America, 5–9% in Europe, and 1-5% in Asia[3], PCNL is not performed as frequently as one might expect. This discrepancy can be attributed to the considerable level of expertise and technical skills required for the procedure. It has been estimated that surgeons require from 45 to 105 operations to achieve competence and excellence, respectively, in performing the procedure[4–6]. As a result, many surgeons and healthcare facilities opt for alternative approaches, such as Retrograde Intrarenal Surgery (RIRS) or Shock Wave Lithotripsy. In such cases, patients do not receive the optimal procedure, leading to longer operation time, higher costs, lower stone clearance rate and longer hospitalization[7,8].

Over the past decade, several research projects and studies have explored the use of robotic systems and augmented reality (AR) to enhance precision and safety during PCNL procedures[9]. These advancements aim to support surgeons in the most challenging part of the procedure - the renal access - reducing the risks associated with manual techniques and the level of expertise required to perform this type of surgery. Due to the percutaneous nature of PCNL, surgeons lack direct visualization of the target organ and surgical instruments. AR provides valuable advantages by offering an enhanced view of the surgical field, such as overlaying a 3D anatomical model of the organs onto the patient's body, improving spatial orientation and procedural accuracy. In studies like[10] and ref. 11, AR systems are used to overlay a 3D model onto the image from a tablet camera, providing surgeons with additional and helpful information about the patient's anatomy. Robotic-assisted systems like PAKY[12] offer an alternative for precise percutaneous access, enabling more accurate needle placement into the kidney and ensuring no deviation from a safe trajectory. Recently, several studies have introduced ultrasound-guided robotic systems[13]. Typically, these systems feature a surgical needle mounted on a robotic arm, controlled either automatically or via teleoperation within a 3D or 2D imaging volume. Li et al. have proposed a collaborative robotic system to assist the surgeon in positioning the ultrasound probe while compensating for respiratory motion[14]. Once positioned, the system proceeds with needle insertion. Recent works combine AR and robotic assistance, merging the strengths of both technologies. Fu et al.[15] developed an innovative system that integrates robotic assistance with augmented reality to support surgeons in aligning the needle to a pre-planned trajectory and maintaining it with the help of a collaborative robot during the puncture phase, yielding highly promising results in experimental testing. Meanwhile, Yang et al.[16] designed a robot-assisted tele-ultrasound diagnositc system utilizing 5G technology, enabling real-time ultrasound navigation and allowing remote diagnostic capabilities, thus expanding access to specialist care across distances. Early integration of AR and robotics in PCNL was presented in ref. 17, although the system lacked real surgeon validation, relied on external markers for registration, and did not incorporate real-time ultrasound guidance, limiting its clinical

[1]Department of Sciences and Methods for Engineering, University of Modena and Reggio Emilia, Reggio Emilia, Italy. [2]Surgical, Medical and Dental Department of Morphological Sciences related to Transplant, Oncology and Regenerative Medicine, University of Modena and Reggio Emilia, Modena, Italy. [3]Azienda Ospedaliero-Universitaria di Modena, Policlinico di Modena, Modena, Italy. ✉e-mail: stefano.bazzani@unimore.it

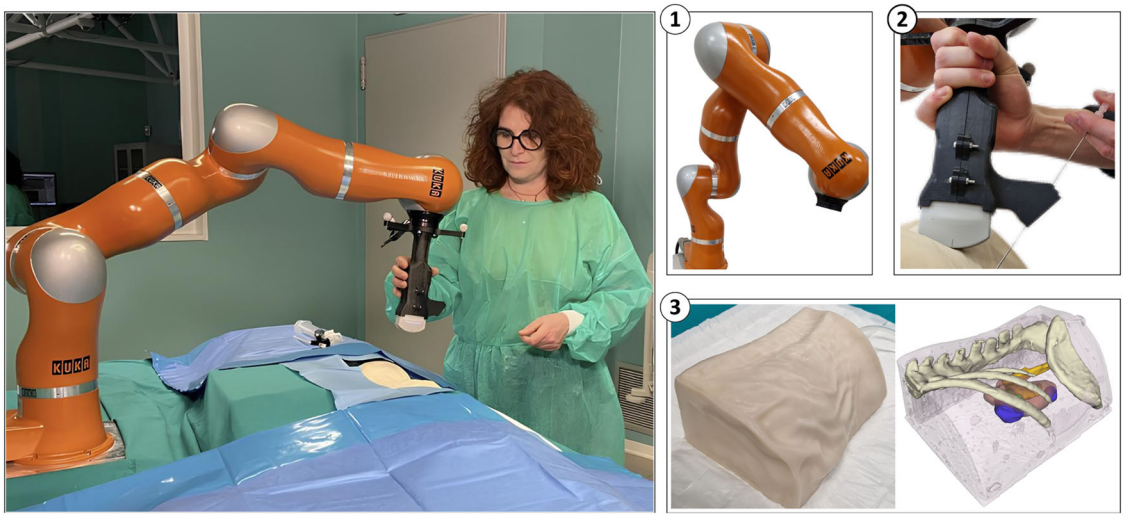

Fig. 1 | System setup. The setup includes: (1) the collaborative robot, (2) the ultrasound probe holder with needle guide, and (3) the abdominal phantom used for system validation. The phantom was also used for the 3D reconstruction, built from its CT scan.

applicability. Recent advances include the work of Taguchi et al.[18] which introduced the first robot-guided, purely radiological renal puncture system approved for clinical use. However, its implementation necessitates intraoperative fluoroscopy. Several commercial products, such as GE Healthcare's Percunav[19], Quantum Surgical's Epione[20], and Massmec's Sirio[21], offer either robotic assistance or ultrasound navigation for percutaneous procedures, particularly in interventional radiology. However, no single system integrates both functionalities, limiting their versatility. Moreover, many of these systems rely on intraoperative CT imaging, which increases patient radiation exposure and necessitates specialized operating rooms, hindering their accessibility in standard surgical settings.

This work aims to overcome the limitations of existing solutions by developing a system that combines robotic assistance, ultrasound navigation, and augmented reality. The proposed integrated approach is designed to reduce the risks associated with renal access during PCNL and to make the procedure accessible to residents and less-experienced surgeons. In particular, the main contribution of this paper are:

- Design and implementation of a system that enables accurate puncture for kidney access by combining 3D anatomical modeling with real-time ultrasound guidance. This allows novice surgeons to gain confidence in executing the initial puncture without relying on fluoroscopic imaging or intraoperative CT scans, thereby minimizing radiation exposure. This advancement could improve procedural safety and broaden the range of medical professionals capable of performing PCNL (and other percutaneous procedures) effectively.
- Optimal pre-operative planning and real-time CT-US registration with needle tracking.
- An extensive validation campaign was conducted in a controlled clinical simulation environment. The validation process involved two phases: (1) Four experienced urologists performed PCNL procedures on a human abdomen phantom, both with and without the aid of the proposed system. Their performance served as a benchmark for comparison. (2) Thirteen residents from the School of Specialization in Urology at the University of Modena and Reggio Emilia replicated the procedures, and their results were compared to the benchmark, both quantitatively and qualitatively.
- Although the paper is focused on the PCNL procedure, the methodology and the developed system may also be exploited in other medical fields, such as for example interventional radiology.

Results

The proposed system for ultrasonographic-guided robotic-assisted PCNL is designed to specifically address the most critical phase of a PCNL procedure: achieving renal access through insertion of a hollow needle into one of the renal calyxes of the kidney. The system is specifically designed for prone PCNL, optimizing US guidance and registration for this patient positioning. However, as described in *Method* section, the system relies on a registration algorithm that produces a transformation matrix ensuring alignment between the CT and US images, regardless of the patient's posture. Thus, it could be easily extended for supine PCNL.

The system, shown in Fig. 1, includes a collaborative robot with 7 degrees of freedom. This robot is equipped with a custom-designed handle that maintains alignment between an ultrasound probe and the PCNL needle through a needle-guide device. The needle-guide offers two selectable inclinations (20 and 30 degrees) relative to the ultrasound probe. The selection of 20 and 30-degrees needle insertion angles is based on current clinical practice in US-guided PCNL procedures. Indeed, these angles provide a wider view for reaching the calyx fornix with the needle. Moreover, these angles align well with the natural posterior angulation of the renal calyces in the prone position, allowing the needle to achieve an easy access through the dorsal calyx group into the renal pelvis[22]. Finally, these angles likely represent a balance between effective kidney access, minimizing risks to surrounding structures, and optimizing the trajectory for subsequent steps of the PCNL procedures. An easy-to-use human-machine interface (HMI) manages the entire system, displayed directly on the operating room monitor. An external tracking system is used to monitor the needle handle and estimate the needle tip position. This information is then used to visualize the needle's path during insertion directly on the ultrasound image displayed within HMI. For validation purposes, the system has been installed within a simulated operating room and assessed by experienced urologists and urology residents in an experimental study. The validation has been performed on a synthetic phantom replicating the human left flank, as depicted in Fig. 1. This phantom incorporates skin, muscle, spine, three ribs, a kidney with upper and lower tumors, a ureter, and a hollow renal pelvis with calyces containing a partial staghorn calculus. The inclusion of tumors into the phantom anticipates the future application of this system for other procedures, such as cryoablation or radiofrequency ablation of tumors. Indeed, the same needle used for initiating PCNL before dilation is exploited even for nephrostomy placement, thermal ablation of renal lesions, but also in interventional radiology procedures like gallbladder drainage and drainage of various intra-abdominal or prostatic abscesses.

The proposed system architecture, depicted in Fig. 2, comprises a robotic system designed to assist and guide the surgeon for optimal execution of the procedure. Specifically, two distinct phases are involved in each surgical intervention: a pre-operative phase and an intra-operative phase.

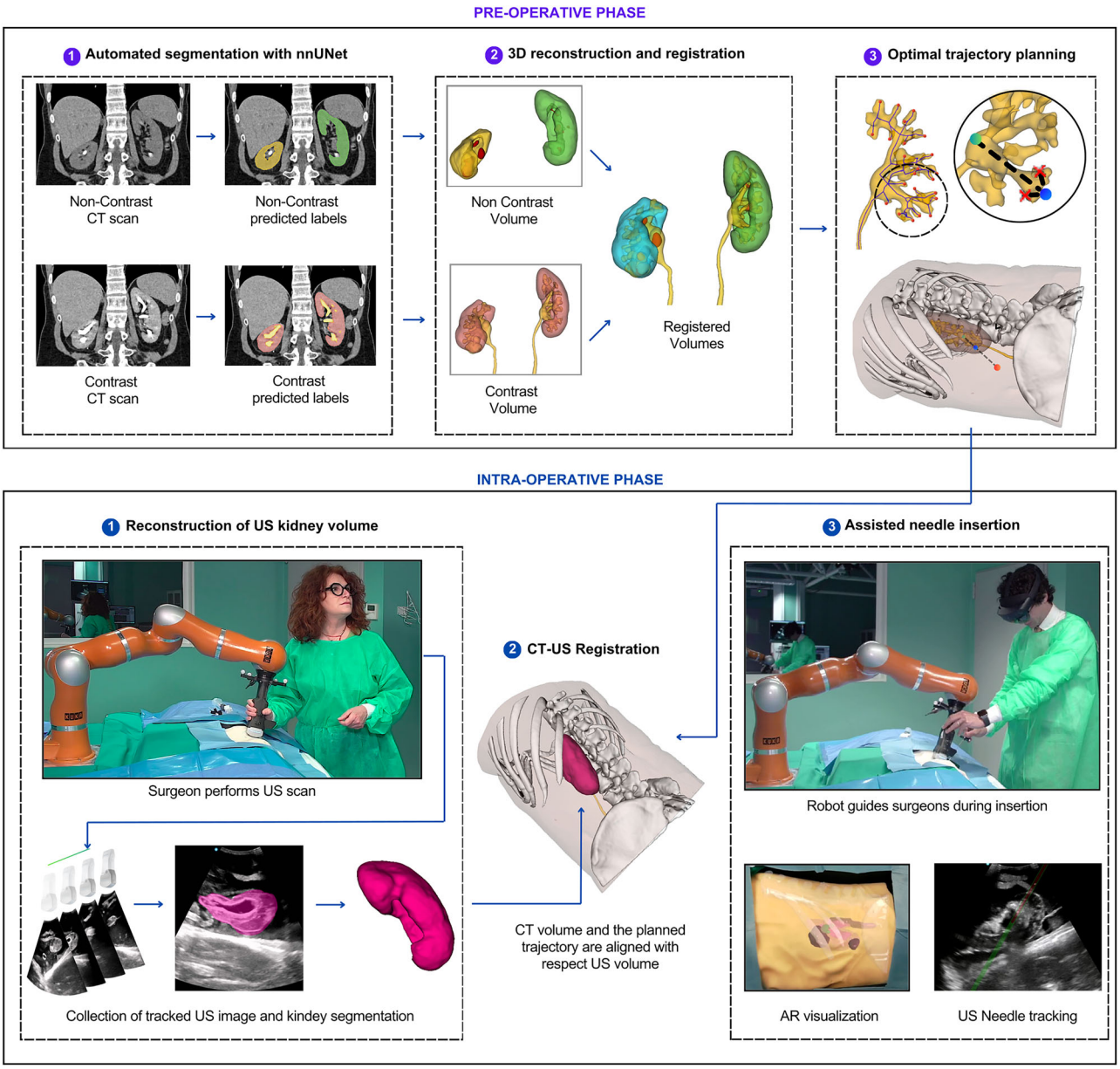

Fig. 2 | Overall system architecture. In the pre-operative phase the optimal trajectory for needle insertion is planned, while in the intra-operative phase the surgeon performs the surgery with the aid of the robotic system.

- *Pre-operative phase*: During this phase, the patient undergoes a Computed Tomography (CT) or Magnetic Resonance Imaging (MRI) scan. The surgeon then utilizes these CT/MRI images for surgical planning. The proposed system offers assistance to the surgeon in this phase by automatically reconstructing a 3D model of the patient's anatomy from the CT/MRI scans. This 3D model serves a dual purpose: it provides the surgeon with a clear visualization of the clinical situation, and it allows the robotic system to compute the optimal needle trajectory for reaching the target calyx.
- *Intra-operative phase*: In this phase, the surgeon performs the surgery with the aid of the robotic system, which guides him/her in maintaining the needle along the pre-planned optimal trajectory. A crucial step in this phase is the CT-US registration, where the reconstructed 3D volume and the pre-planned needle trajectory are aligned with the patient's organs in real-time. This alignment is achieved by merging CT scans with a volume derived from an initial US scan acquired by the surgeon. To provide comprehensive surgical assistance, the technical capabilities of the proposed robotic system are integrated with an AR visualization.

The experimental study was conducted as follows. First, four experienced urologists (three male, one female), all experts in standard PCNL, performed the procedure on the phantom replicating the human abdomen. The procedure was performed manually first to establish a baseline for validation and benchmarking, and then again with the assistance of the robotic system. Subsequently, thirteen residents (six male, seven female) aged between 26 and 30 years old, performed the same procedure on the phantom, both manually and with robotic assistance. During manual execution of the procedure, surgeons were instructed to manually insert through the skin the 18G needle used in PCNL procedures to establish renal access and initiate the procedure before dilation. This insertion was guided by ultrasound. The insertion was considered successful if it punctured the fornix of the renal calyx and allowed previously injected water within the ureter to flow out through the needle. During the robotic-assisted procedure, the system automatically calculated the optimal trajectory for needle insertion and the corresponding positioning of the ultrasound probe. The robot then guided the surgeon's hand to follow this trajectory, ensuring accurate placement of the US probe. With the probe in position, the surgeon

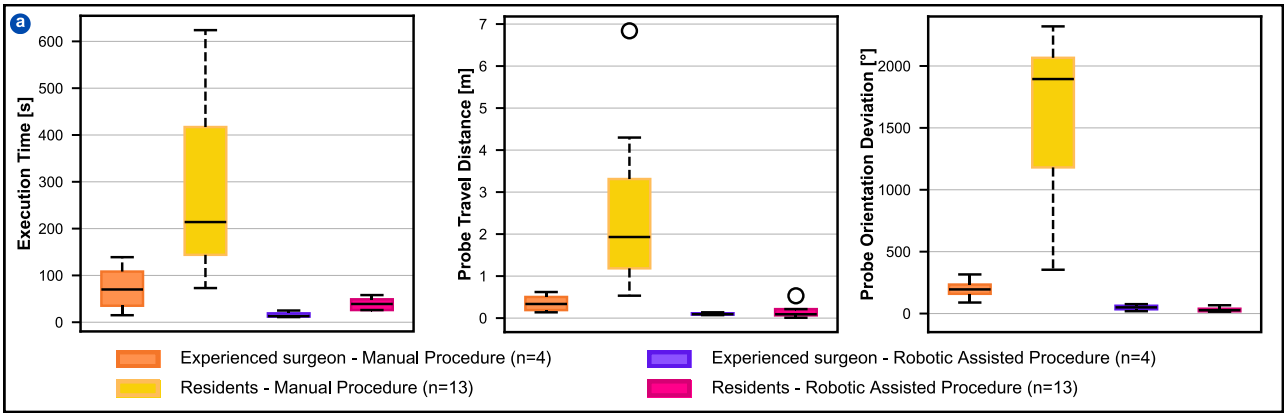

b

	Execution Time	Probe Travel Distance	Probe Orientation Deviation
Manual Procedure Experienced Surgeons vs Residents	t = 3.457 p = 0.0039 ✓	t = 3.920 p = 0.0021 ✓	t = 4.208 p = 0.0014 ✓
Robotic Assisted Procedure Experienced Surgeons vs Residents	t = 3.030 p = 0.0231 ✓	t = 0.853 p = 0.4383 ✗	t = -0.797 p = 0.4780 ✗
Experienced Surgeons Manual Procedure vs Robotic Assisted Procedure	t = 2.028 p = 0.1313 ✗	t = 2.255 p = 0.1043 ✗	t = 3.041 p = 0.0424 ✓
Residents Manual Procedure vs Robotic Assisted Procedure	t = 4.438 p = 0.0009 ✓	t = 4.276 p = 0.0011 ✓	t = 4.646 p = 0.0007 ✓

✓ *statistically significant difference* ✗ *NOT statistically significant difference*

c

		Number of failed punctures												
Experienced Surgeons (n=4)	Manual Procedure	0	0	0	1									
	Robotic Assisted Procedure	0	0	0	0									
Residents (n=13)	Manual Procedure	3	2	2	0	0	1	1	1	0	1	2	1	2
	Robotic Assisted Procedure	0	0	0	0	0	0	0	0	0	0	0	0	0

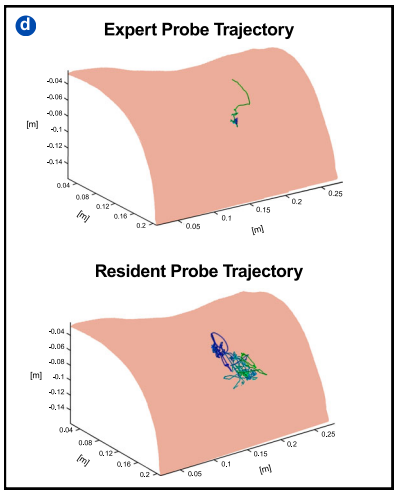

Fig. 3 | Comparison of residents and experienced surgeons. a Comparison in terms of execution time, probe travel distance, and probe orientation deviation. Variability is represented using boxplots, where each box summarizes a set of independent experimental measurements, and the spread of the data reflects the interquartile range, with whiskers extending to the most extreme data points not considered outliers. Middle line represent the median. **b** Results of the independent two-sample *t*-test. **c** Analysis of failed needle insertions. **d** Example of probe trajectory differences between an experienced surgeon and a resident.

could then insert the needle through the needle-guide directly attached to the US probe holder.

The Supplementary Video 1 shows and describes the system for ultrasonographic-guided robotic-assisted PCNL, while in the following sections the results of the experimental campaign are presented.

Performance evaluation

The evaluation of the experimental data focused on comparing the performance of the manual and robotic-assisted procedures. The performance of experienced surgeons served as the ground truth for this comparison. In the following, box plots are used as the visual tool to summarize the quantitative results. We collected data on two key metrics: procedure execution time and precision in achieving renal access. Renal access refers to reaching the fornix of the targeted calyx while avoiding nearby organs. An independent two-sample *t*-test employing Welch's correction for unequal variances was applied to evaluate the quantitative results obtained during the experimental campaign. This was done to determine the statistical significance of the difference between the groups. Statistical significance is assessed when $p < 0.05$. Table in Fig. 3b lists the *t*-values and *p*-values that resulted from the statistical analysis. In particular, for each metric we assessed differences between residents and experienced surgeons, and between manual and robotic assisted procedures.

Figure 3a specifically compares procedure execution times between experienced surgeons (orange: manual, violet: robotic-assisted) and residents (yellow: manual, pink: robotic-assisted). As the figure reveals, robotic assistance appears to reduce variability in the data, particularly for residents. This is evident by the narrower box plot for the residents performing the robotic-assisted procedure compared to the manual procedure, a finding further confirmed by the statistical analysis, which reveals a significant difference in residents' execution time when comparing the two approaches. This finding supports the potential of robotic assistance to mitigate the high execution times typically observed among residents performing manual procedures. For instance, the average time required for residents to complete the manual procedure was 290 s (with a median of 214 s), whereas experienced surgeons completed it in just 73 s (median of 70 s). The results are completely leveraged in the case of robotic-assisted procedures, where the completion times for both residents and experienced surgeons are very similar and exhibit minimal variability. Nevertheless, statistical analysis indicates a significant difference in the execution time of robotic-assisted procedures when comparing experienced surgeons and residents. This finding is likely influenced by the small sample size and may be attributed to the greater confidence and consequent speed of experienced surgeons during the procedure, while residents might exhibit more caution, even with the aid of the robot.

The second metric that we explored is the precision in achieving renal access. At first, we focused on needle placement accuracy and we evaluated the number of failed needle insertions. In the experiment, a failed insertion was defined as:

- Missing the fornix: The needle tip failed to reach the fornix of the targeted calyx, after positioning the ultrasound probe in the supposed optimal location.

- Puncturing forbidden regions: The needle accidentally punctured a nearby organ that should be avoided.Figure 3c summarizes the number of failed insertions for residents and experienced surgeons during both manual and robotic-assisted procedures. The table reveals a clear trend: residents generally encountered failed insertions (sometimes multiple) in the manual procedure, while experienced surgeons made only one error. Notably, no failures occurred during the robotic-assisted procedure for either group. This suggests that the robotic system improves performance not only for residents, as expected, but also for experienced surgeons.

Then, we evaluated the distance traveled by the ultrasound probe and the changes in its orientation (Fig. 3a) before reaching the target point on the skin for the subsequent insertion. The total orientation deviation is computed by summing the axis-angle rotations executed by the probe around its principal axis at each instant during the search for the insertion pose. The reader is referred to ref. 23 for detailed information regarding the axis-angle representation. These metrics allow us to understand how long the search for the target point has taken, as the greater the distance traveled and the change of orientation, the greater the uncertainty in finding the optimal insertion point. As is evident from the quantitative data shown in the figure, in the manual procedure the distances traveled by the US probe and the orientation deviations were very short for the experienced surgeons (orange plot), showing confidence in finding the positioning. On the other hand, the residents were more uncertain (yellow plot), indeed the distances traveled reached very high values (average distance: 2.46 m, median: 1.93 m), decidedly higher than those of the experienced surgeons (average distance: 0.35 m, median: 0.34 m), as far as the orientation deviations (average orientation deviation: 1906 degrees, median: 1895 degrees for residents, compared to average orientation deviation: 199 degrees, median: 195 degrees for experienced surgeons). As for the robot-assisted procedure (violet and pink plots), instead, once again the system allowed the result to be leveled and both experienced surgeons and residents reached the optimal position with a very short path and with little orientation deviation. The statistical analysis supported all findings related to probe travel distance and orientation deviation, revealing a significant difference between experts and residents in the manual procedure. Additionally, residents showed a significant enhancement in performance when utilizing the robotic-assisted approach compared to the manual technique. Notably, experienced surgeons exhibited a significant improvement solely in orientation, the most challenging aspect, suggesting the robot's utility even for this group.

Finally, we visualized the trajectories of the ultrasound probe in the manual procedures executed by residents and experienced surgeons. Figure 3d shows an example of this visualization, where the previously described trend is clearly confirmed.

Usability

The effort required to use a system or a device defines its usability. In order to state that the use of the robotic system makes the procedure more usable with respect to the execution of the procedure manually, without robotic assistance, we conducted a statistical analysis adopting a surgery-specific version of the NASA Task Load Index (NASA-TLX) questionnaire[24]: the Surgeon Task Load Index (SURG-TLX)[25]. It provides a multidimensional surgeon's workload measure, reflecting the specific demands of the surgical environments[11], framed into six subscales (i.e., Mental Demands, Physical Demands, Temporal Demands, Task Complexity, Situational Stress and Distractions). Based on ref. 17, for the current investigation, only the raw data of the SURG-TLX were considered, since it has been shown that it might increase the experimental validity. The questionnaire was administered to the participating surgeons after having performed the tests, as suggested by the experiences of Yu et al.[26]. Figure 4 reports the mean values of the SURG-TLX for both the manual experiments and the robot-assisted experiments, executed by the experienced surgeons and the residents. Plot values represent effort levels expressed as percentages, ranging from 0% (no effort) to 100% (maximum effort). Analysis of the data reveals two primary trends:

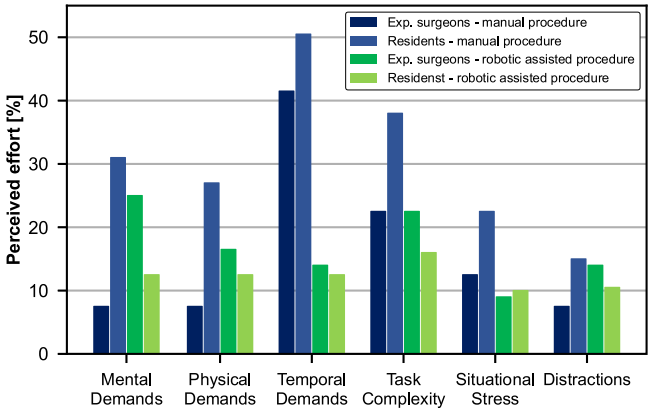

Fig. 4 | Results of the SURG-TLX questionnaires.

- Robotic assistance (green columns) generally decreases effort compared to manual procedures (blue columns). However, in certain cases, experienced surgeons reported higher effort levels with the robotic system. This might be due to their familiarity with manual techniques, where adapting to robotic systems initially demands increased effort.
- Manual procedures (blue columns) show a considerable discrepancy between effort reported by residents and that observed by experienced surgeons. The implementation of robotic assistance significantly narrows this gap, bringing residents' perceived effort closer to that of experienced surgeons (green columns).In conclusion, the introduction of robotic systems offers several advantages, particularly for residents.

Discussion

In this study, we present a robotic system designed to assist surgeons during PCNL procedures. A critical challenge in PCNL is achieving precise renal access while avoiding damage to surrounding organs and structures. The proposed system automates pre-operative planning by calculating the optimal needle trajectory for reaching the target calyx and guides the surgeon in maintaining the needle along the pre-planned optimal trajectory. The system is designed for prone PCNL. However, since it relies on the CT-US registration algorithm, the system could be easily extended for supine PCNL, expanding its applicability to different surgical approaches. To aid the initial guess of the registration algorithm, acquiring the CT in an orientation similar to that of the procedure (e.g., acquiring the CT in a prone position if the procedure is executed prone) could be helpful.

The proposed system advances state-of-the-art techniques by combining 3D anatomical modeling with real-time ultrasound guidance. This eliminates the need for radiation-intensive imaging modalities, such as fluoroscopy and intra-operative CT scans, while enabling accurate pre-operative planning, real-time CT-US registration, and needle tracking. By integrating pre-operative and intra-operative information, surgical accuracy is enhanced. While the proposed ultrasound-guided technique eliminates intra-operative radiation exposure (CT/MRI, X-ray), the reliance on a pre-operative CT scan does partially diminish the overall radiation exposure benefit for the patient. However, the pre-operative CT scan is an essential diagnostic examination for defining the pathology and planning the treatment. The proposed approach does not introduce new radiation exposure but builds upon an examination already required within the standard diagnostic pathway. Accurate CT-US registration is essential to ensure adherence to the pre-planned trajectory and, consequently, the effective operation of the system. Currently, registration accuracy is qualitatively assessed through visual inspection by experienced surgeons. However, in the near future, we will integrate two additional features to quantitatively evaluate CT-US registration accuracy: first, we will compare the intra-operative kidney point cloud generated from the US scans with the pre-operative kidney volume reconstructed from the CT by computing point-to-surface distances. This metric will provide an estimate of spatial

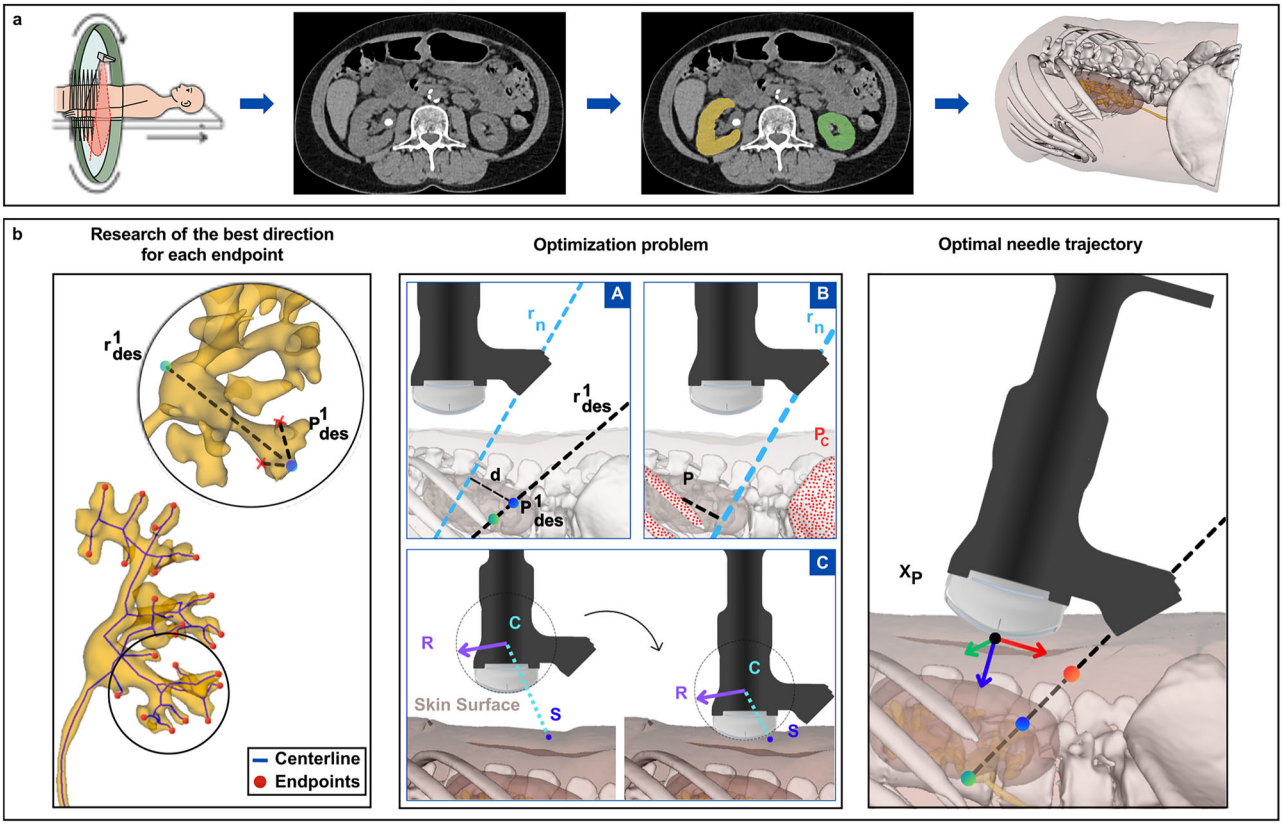

Fig. 5 | Pre-operative phase. a Starting from a CT or MRI scan, the segmentation and 3D reconstruction of the relevant anatomical structures is executed. **b** The optimal and safe needle trajectory for reaching the target calyx is computed as the solution to an optimization problem with constraints A, B, and C.

alignment. Second, we will consider integrating an electromagnetic (EM) needle to evaluate the error between the pre-planned target position and the actual one.

A controlled clinical simulation involving four experienced surgeons and thirteen residents demonstrated the effectiveness of the proposed system. The system improved precision in renal access, reduced procedure time, and enhanced usability for all participants. Importantly, residents achieved performance comparable to experienced surgeons, suggesting that the system can empower a wider range of medical professionals to perform PCNL and other percutaneous procedures effectively. The proposed system's versatility allows for adaptation to other needle-based procedures, including biopsies and interventional radiology techniques like nephrostomy, renal ablation, cholecystostomy, and percutaneous drainage of intra-abdominal or prostatic abscesses. Given that the same needle is used in both PCNL initiation before dilation and these procedures, the system can be customized by fine-tuning parameters for optimal trajectory planning in each specific procedure. Therefore, future work will focus on extending the AR and robotic system to other procedures, such as liver punctures for ablation techniques (MWA, RFA). By enabling precise needle guidance, the system will allow avoiding critical structures in complex anatomical areas, such as the hepatic dome. While liver interventions present unique challenges due to the liver's high degree of deformability, these challenges will be carefully considered in future developments.

Intra-operative patient movements are not currently handled by the proposed system. After registration, maintaining patient immobility is crucial, a task complicated by respiratory motion. However, leveraging the fact that PCNL is traditionally performed under general anesthesia[27], a practical solution involves mechanically inducing a brief apnea before ultrasound acquisition and maintaining it throughout the needle insertion process (computation, positioning, and puncturing), which is completed within a minute. The inherent safe apnea period for a healthy individual breathing room air is around 1 min and can be extended through preoxygenation or a high fraction of inspired oxygen[28]. Future work will aim to integrate respiratory motion compensation, exploring techniques similar to those described in ref. 14.

Methods

In the pre-operative phase, the patient undergoes a CT or MRI scan. After a predetermined time interval, a contrast liquid is injected. The proposed system leverages both the non-contrast (base phase) and contrast-enhanced (arterial, portal venous and late phases) CT/MRI scans to perform the following tasks automatically:

- Segmentation and 3D reconstruction of the relevant anatomical structures: kidney stones, renal parenchyma, calyces, and ureter (Fig. 5a).
- Computation of an optimal and safe needle trajectory for reaching the target calyx (Fig. 5b).

In the intra-operative phase, the surgeon performs the procedure with the assistance of the robotic system. The robot guides the surgeon in maintaining the probe in the pre-planned pose, ensuring optimal needle insertion trajectory. The intra-operative phase consists of the following steps:

- CT-US registration: The reconstructed 3D volume and the pre-planned needle trajectory and US probe location are aligned with the patient's organs in real-time by merging CT scans with a volume calculated from an initial US scan performed by the surgeon (Fig. 6a).
- Robot assistance to guide the surgeon towards the US probe location that corresponds to the optimal needle insertion trajectory (Fig. 6b).
- Manual execution of the needle insertion through the needle-guide executed manually by the surgeon (Fig. 6c).
- Needle tracking: visual feedback of the needle's trajectory is provided to the surgeon to verify correct needle insertion (Fig. 6d).

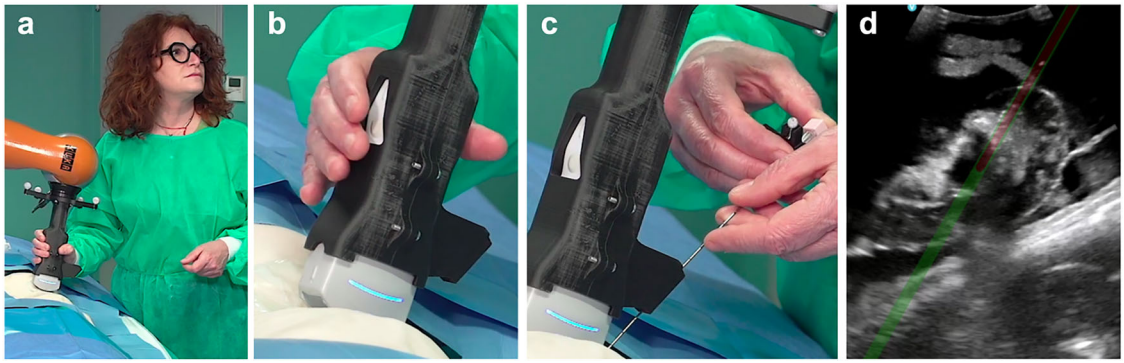

Fig. 6 | Intra-operative phase. The surgeon executes an initial US scan (**a**). Then, a registration algorithms performs the alignment between the pre-operative information and the organs of the patients. The robot guides the surgeon to position the probe in the optimal pose (**b**) to execute the needle insertion. **c** During the insertion a needle tracking algorithm provides a visual feedback (**d**).

In the following, a description of each pre- and intra-operative step is provided. All individuals in identifiable images have released signed informed consent for publication.

Automated segmentation and 3D reconstruction

The first step, shown in Fig. 5a, involves automatically segmenting and reconstructing kidney stones and anatomical structures from CT/MRI scans. We implemented a neural network-based architecture to segment and register the CT/MRI images.

Segmentation aims to automatically identify different anatomical parts in CT/MRI images, based on the various scan phases. Specifically, we implemented two pre-trained U-Net models[29]. These models segment the kidney parenchyma and stones from non-contrast CT scans, and the kidney parenchyma, ureter, and calyces from late-phase CT scans. The first model is trained on a dataset of 125 non-contrast CT scans (split into 100 for training and 25 for testing). Similarly, the second model is trained on a dataset of 60 late-phase contrast CT scans (divided into 50 for training and 10 for testing). Additionally, the same architecture can be used to extract arteries and veins from the arterial and portal venous phases, respectively. By applying a threshold algorithm based on Hounsfield Units to the entire volume, we also segmented bones and skin.

Since reference frames of non-contrast and contrast CT scans may differ, the labels generated by the two models require alignment (registration). To achieve this, we leveraged the kidney parenchyma, segmented by both models, to align the CT phases. This resulted in a single, unified 3D model.

Identification of the target calyx

During PCNL, achieving renal access involves inserting the hollow needle into a renal calyx of the kidney. Thus, the second step in the pre-operative phase is determining the optimal needle trajectory. This requires two key actions: first, the system must automatically identify the target calyx, including the needle insertion point and the optimal insertion angle, and second, it needs to compute a safe path that reaches the fornix of the selected calyx while avoiding nearby organs.

In order to compute the needle insertion point and the insertion angle, the pre-operative planner processes the 3D calyces surface and extract the centerline, to identify all the calyces branches and their endpoints, as shown in Fig. 5b (left). Then, the planner selects all points within a geometric neighborhood of the endpoints as potential needle insertion points. For each candidate point, a line bundle is generated, and the line maximizing needle penetration into the calyces is chosen. A single point-line pair is thus determined for each neighborhood. The resulting list of candidate insertion points $\mathcal{P} = \{\mathbf{P}^1_{\text{des}}, \mathbf{P}^2_{\text{des}}, \ldots, \mathbf{P}^n_{\text{des}}\}$, where $\mathbf{P}^i_{\text{des}} \in \mathbb{R}^3$, with corresponding inclination of the lines $\mathcal{R} = \{\mathbf{r}^1_{\text{des}}, \mathbf{r}^2_{\text{des}}, \ldots, \mathbf{r}^n_{\text{des}}\}$, where $\mathbf{r}^i_{\text{des}} \in \mathbb{R}^3$, is sorted by decreasing depth of potential needle insertion within the calyceal volume.

Computation of the desired optimal trajectory

The goal is to select the needle inclination for maximum calyx penetration depth. Indeed, this inclination corresponds to a trajectory that is as perpendicular as possible to the fornix of the calyx, thereby minimizing the risk of lateral calyx exit. Therefore, the pair of point and inclination $(\mathbf{P}^1_{\text{des}}, \mathbf{r}^1_{\text{des}})$ within the sorted list $\mathcal{P}$ represents the desired candidate for computing the trajectory of the needle.

Since the needle is inserted through a guide mechanically connected to the ultrasound probe, a US probe position and orientation (pose), $\mathbf{x}_p \in \mathbb{R}^6$, can be calculated to guarantee the needle follows the desired path. This calculation must also incorporate additional constraints to ensure a safe trajectory:

- The needle path must avoid critical structures such as organs (e.g., colon) and bones (e.g., ribs).
- The ultrasound probe must maintain tangential contact with the patient's skin. This is essential for real-time ultrasound imaging, providing the surgeon with visual feedback as the needle is inserted.

To achieve a trajectory fulfilling all these conditions, as shown in Fig. 5b (center and right), the following optimization problem was formulated.

$$\min_{\mathbf{x}_p} \quad f(\mathbf{x}_p) = 1 - |\mathbf{r}^1_{\text{des}} \cdot \mathbf{r}_n(\mathbf{x}_p)| \tag{1a}$$

$$\text{subject to} \quad d(\mathbf{r}_n(\mathbf{x}_p), \mathbf{P}^1_{\text{des}}) = 0, \tag{1b}$$

$$\forall \mathbf{P} \in \mathcal{P}_c \; d(\mathbf{r}_n(\mathbf{x}_p), \mathbf{P}) > \varepsilon \tag{1c}$$

$$\exists \mathbf{S} \in \mathcal{S}_c \quad \text{such that} \quad d(\mathbf{C}, \mathbf{S}) = R - \delta. \tag{1d}$$

The probe pose $\mathbf{x}_p$ is chosen as optimization variable. Indeed, given $\mathbf{x}_p$ and thanks to the mechanical coupling between the US probe and the needle-guide, it is possible compute the orientation of the needle $\mathbf{r}_n(\mathbf{x}_p)$ and verify that it respects all the constraints.

The optimization problem is supplied with inputs including the 3D volumes of the body and skeleton obtained during the reconstruction phase, as well as the outputs generated by the algorithm for computing the insertion point and inclination. The minimization function is designed to align the needle angle with the desired orientation $\mathbf{r}^i_{\text{des}}$ (1a). The function $f(\mathbf{x}_p)$ represents the angular difference between the linear path of the needle through the needle-guide and the desired angular orientation. By minimizing this function to approach zero, the two lines will become parallel.

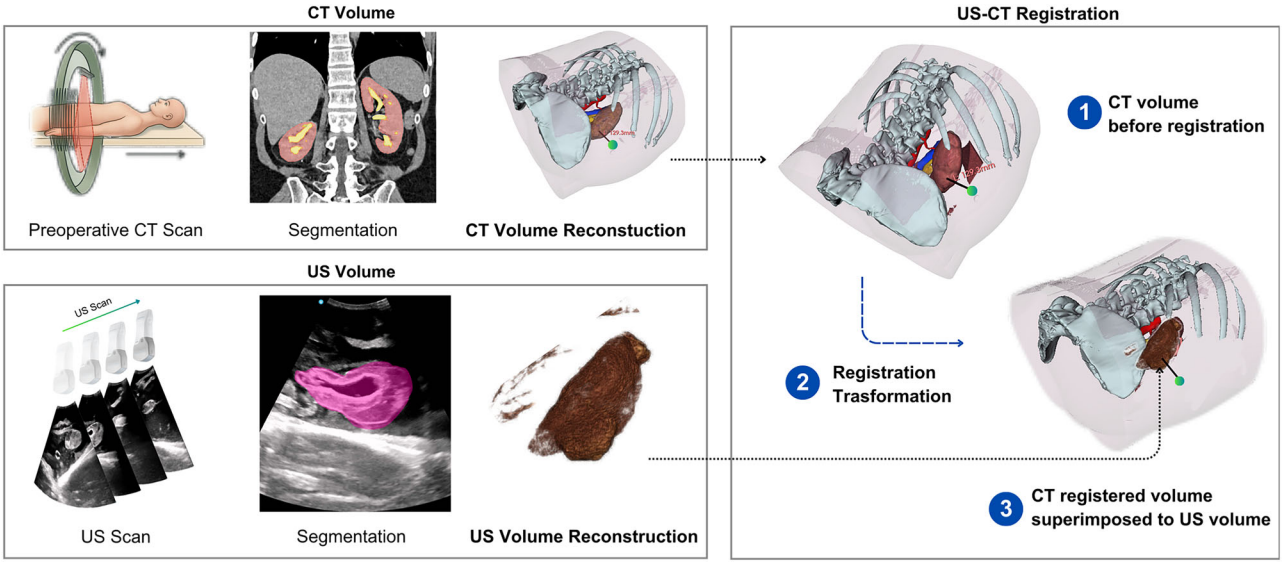

Fig. 7 | Real-time registration process to intra-operatively align the reconstructed model and the optimal needle trajectory with the patient's anatomy.

Beyond ensuring the correct needle angle, it is essential that the needle trajectory intersects the target insertion point in the calyx surface identified by the algorithm described in the previous paragraph. This requirement is formalized as the constraint (1b) within the optimization problem, ensuring that the distance between the desired intersection point $\mathbf{P}^1_{\text{des}}$ and the needle line $\mathbf{r}_n(\mathbf{x}_p)$ is zero (Fig. 5b-A).

Then, the needle path must avoid critical structures such as organs and bones. To this aim, the constraint (1c) is formulated. By merging the point clouds of the organs and areas to be avoided, a single point cloud $\mathcal{P}_c$ is obtained. The constraint ensures that the needle trajectory maintains a safe distance $\varepsilon > 0$ from all points $\mathbf{P} \in \mathbb{R}^3$ in P_c (Fig. 5b-B).

Finally, the constraint (1d) of the optimization problem guarantees the tangency between the probe and patient skin. Given that the probe's terminal part is an arc of a circle, we can calculate its center $\mathbf{C} \in \mathbb{R}^3$ and its radius $R \in \mathbb{R}$ (Fig. 5b-C). To ensure full contact and firm pressure for a clear ultrasound image, we impose the condition that there must exist at least one point $\mathbf{S} \in \mathbb{R}^3$ of the skin point cloud $\mathcal{S}_c$ such that the distance between $\mathbf{S}$ and $\mathbf{C}$ is equal to $R - \delta$, where $\delta = 0.5$ cm. If the optimization process fails to converge, a new iteration begins by selecting the next insertion point-inclination pair from the sorted list.

CT-US registration

The optimal needle trajectory determined during the pre-operative phase is calculated based on a CT scan performed a few days before the actual surgical intervention. During the intervention, the patient's position and environmental conditions may differ substantially from the pre-operative situation. Therefore, real-time registration is necessary to intra-operatively align the reconstructed model and the optimal needle trajectory with the patient's organs (Fig. 7).

To achieve this, a registration process consisting of the following phases is applied:

- The surgeon performs an initial US scan to explore the patient's region of interest. During this procedure, the US images and the pose of the probe are acquired. A deep learning-based architecture, such as the one described in ref. 30, is exploited to perform kidney segmentation within each US image. By leveraging the knowledge of US image position and orientation, a 3D US volume of the kidney is reconstructed by merging all the kidney pixel segments.
- A CT-US registration algorithm, fed with both 3D CT and US kidney volumes, is applied to align these volumes. The algorithm involves an optimization problem that minimizes the distance between points in the CT volume and their corresponding points in the US volume. The output of the algorithm is a transformation matrix that specifies the translational and rotational adjustments required to align the CT volume with the US volume.
- The transformation matrix is then applied to the CT volume. This operation ensures that all computations and results obtained during the pre-operative phase are accurately translated to correspond with the patient's actual position on the operating table.

Robotic-assisted US probe placement and needle insertion

Once registration is completed, the robot knows the probe target pose, that is the one that allows the optimal needle insertion. To enable physical interaction between surgeon and robot, we employed a collaborative robot and implemented an impedance control running at a frequency of 500 Hz. This approach allows the robot to behave compliantly with the surgeon's movements, according to a mass-spring-damper system. For in-depth technical details on impedance control, the reader is referred to ref. 31. The robot then acts as a gentle assistant guiding the surgeon towards renal access through the generation of virtual forces, namely virtual fixtures, according to the following scheme:

- From the initial pose to the target pose the robot behaves as a passive supervisor, restricting the surgeon movements by generating virtual forces that allows movements and rotations only towards the target pose, preventing the surgeon to move in other directions (Fig. 6b).
- When the US probe reaches the target pose, the robot behaves as a fixed guide, applying virtual forces on the tool to maintain the needle-guide along the desired path, allowing the surgeon to perform the needle insertion (Fig. 6c).

This approach empowers the surgeon to independently achieve percutaneous access and perform the surgical intervention with the robotic assistance. By ensuring successful and complication-free procedures, especially during the initial learning phase, the system enhances overall surgical performance. The system could even be left evolving autonomously.

Needle tracking

During the insertion phase, the surgeon utilizes the visual feedback from the ultrasound image to visualize the needle tip's location within the patient's body (Fig. 6d). Tracking the needle offers notable advantages by improving puncture precision and enabling surgeons to effectively verify that the target calyx has been reached. Numerous standard algorithms, such as ref. 32, exist for tracking needles within the ultrasound image. However, situations may arise where the needle, or portions of it, are not visible within the ultrasound image plane. In

Fig. 8 | Visualization of the reconstructed model and the planned needle trajectory overlaid on the phantom as seen through the AR headset.

these cases, determining the exact moment when the needle penetrates the inner portion of the renal calyx can become challenging for the surgeon.

To overcome this issue, the system incorporates an external tracking system that monitors both the ultrasound probe and the needle base with a frequency of 120 Hz. Since the needle is inserted through a hole mechanically linked to the probe, maintaining a specific orientation, the needle's trajectory within the ultrasound image is known a priori. Given the knowledge of the needle's length, tracking the needle base enables precise determination of the tip's position relative to the probe and, consequently, its location within the ultrasound image. Due to the constraints imposed by the needle-guide and the insertion point, needle deformation is negligible and is not accounted for in the needle tracking computations. However, needle flexibility could be addressed by integrating an EM tracking needle, a specialized needle equipped with a tiny EM sensor at or near its tip. This sensor interacts with an EM field generated by a separate unit, enabling the precise, real-time tracking of the needle's position and orientation.

These data are input into a custom algorithm that superimposes two visual elements onto the live ultrasound image:

- The trajectory that the needle is expected to follow during the insertion phase (green line in Fig. 6d);
- The real-time position of the needle tip, indicating the portion of the needle that has been inserted. (red line in Fig. 6d).The surgeon can view both the unaltered and the augmented images on separate displays. The surgeon also has the option to toggle the visibility of the added elements, such as the predicted needle trajectory and the needle tip position.

Augmented reality as additional assistance

Preoperative imaging data, such as CT or MRI scans of the anatomical regions of interest, has been extensively exploited to develop Augmented Reality (AR) solutions that enhance surgical capabilities[10,33–35]. For experienced surgeons, augmented reality visualization of renal anatomy has been proved to be sufficient to estimate correct needle angles to reach the target. However, several doubts persist whether residents still need additional technical assistance apart from AR support[10], like the robotic system proposed in this paper. To provide comprehensive surgical assistance, we integrated the technical capabilities of the proposed robotic system with the potential of AR support. The 3D model reconstructed during the pre-operative phase is incorporated into an AR application designed for an AR headset, allowing for direct visualization on the patient's body. The real-time registration process described in *Registration* section ensures accurate intra-operative alignment of the reconstructed model with the patient's anatomy. Figure 8 shows the visualization of the reconstructed model and the planned needle trajectory overlaid on the phantom as seen through the AR headset.

While the AR application is not central to the overall system—the CT-US registration allows the robotic arm to precisely position itself for needle insertion along the pre-planned trajectory - its integration offers valuable visual feedback to the surgeon, especially during the insertion phase. Specifically, during the puncture, the clinician can visualize the estimated needle tip position within the AR model. This relies on a 3D image, unlike the 2D visualization provided by ultrasound alone, thereby enhancing guidance and accuracy. Despite its potential, the clinical application of AR headsets to date still presents the following limitations:

- **Latency issues**. Although the reconstructed model is updated at a nominal frequency of 30 Hz, rapid head movements—such as quick turns—can introduce delays in the adjustment of the model's position and orientation. These momentary lags can disrupt the alignment between virtual and real anatomy, reducing the reliability of AR as a standalone tool for precise intra-operative guidance and feedback.
- **Accuracy**. AR headsets are not designed to achieve high spatial accuracy, which poses further limitations in precision-critical surgical tasks. Quantifying the accuracy of the AR overlay is challenging, but it can be qualitatively estimated based on the surgeon's visual feedback. The precision of the alignment depends largely on the accuracy of the CT-US registration. In the proposed setup, more stable and accurate overlay was achieved by calibrating the AR headset using fiducial markers, such as QR codes, which improved the spatial correspondence between the virtual model and the patient's anatomy.
- **Visual issues**. AR headsets suffer from visual limitations that impact surgical usability. Optical distortions can affect depth perception and spatial accuracy, while parallax errors—caused by head movements—may shift the perceived position of virtual elements. In addition, the limited field of view restricts the amount of overlaid information visible at once, requiring frequent head adjustments to maintain situational awareness.
- **Ergonomy**. Current commercially available headsets lack proper ergonomic design and may not offer sufficient comfort for surgeons, particularly during prolonged procedures, potentially leading to fatigue or reduced concentration.

Data availability

The CT volumes, ultrasound images, and 3D reconstructions of organs and anatomical parts used in this study are available at https://github.com/stefanoBazzani/robotic_assisted_pcnl.

Code availability

The script for automated trajectory planning is available at https://github.com/stefanoBazzani/robotic_assisted_pcnl.

Received: 5 March 2025; Accepted: 12 June 2025;
Published online: 08 July 2025

References

1. Morris, D. S. et al. Temporal trends in the use of percutaneous nephrolithotomy. *J. Urol*. **175**, 1731–1736 (2006).
2. De la Rosette, J. et al. The clinical research office of the endourological society percutaneous nephrolithotomy global study: indications, complications, and outcomes in 5803 patients. *J. Endourol*. **25**, 11–17 (2011).
3. Sorokin, I. et al. Epidemiology of stone disease across the world. *World J. Urol*. **35**, 1301–1320 (2017).

4. Ziaee, S. A. M., Sichani, M. M., Kashi, A. H. & Samzadeh, M. Evaluation of the learning curve for percutaneous nephrolithotomy. *Urol. J.* **7**, 226–231 (2010).
5. Allen, D., O'Brien, T., Tiptaft, R. & Glass, J. Defining the learning curve for percutaneous nephrolithotomy. *J. Endourol.* **19**, 279–282 (2005).
6. Song, Y., Ma, Y., Song, Y. & Fei, X. Evaluating the learning curve for percutaneous nephrolithotomy under total ultrasound guidance. *PloS one* **10**, e0132986 (2015).
7. Srisubat, A., Potisat, S., Lojanapiwat, B., Setthawong, V. & Laopaiboon, M. Extracorporeal shock wave lithotripsy (ESWL) versus percutaneous nephrolithotomy (PCNL) or retrograde intrarenal surgery (RIRS) for kidney stones. *Cochrane Database Syst. Rev.* **8**, CD007044 (2014).
8. Cheng, Y. & Xu, R. Effectiveness and safety of retrograde intrarenal surgery (RIRS) vs. percutaneous nephrolithotomy (pcnl) in the treatment of isolated kidney stones. *Am. J. Transl. Res.* **14**, 1849 (2022).
9. Ferraguti, F., Farsoni, S. & Bonfè, M. Augmented reality and robotic systems for assistance in percutaneous nephrolithotomy procedures: recent advances and future perspectives. *Electronics* **11**, 2984 (2022).
10. Rassweiler, J. J. et al. ipad-assisted percutaneous access to the kidney using marker-based navigation: initial clinical experience. *Eur. Urol.* **61**, 628–631 (2012).
11. Muckler, F. A. & Seven, S. A. Selecting performance measures: "Objective" versus "Subjective" measurement. *Hum. Factors* **34**, 441–455 (1992).
12. Su, L.-M. et al. Robotic percutaneous access to the kidney: comparison with standard manual access. *J. Endourol.* **16**, 471–475 (2002).
13. Cinquin, P. How today's robots work and perspectives for the future. *J. Visc. Surg.* **148**, e12–e18 (2011).
14. Li, H.-Y. et al. Towards to a robotic assisted system for percutaneous nephrolithotomy. In *Proc. IEEE/RSJ International Conference on Intelligent Robots and Systems (IROS)* 791–797 (IEEE, 2018).
15. Fu, J. et al. Augmented reality and human-robot collaboration framework for percutaneous nephrolithotomy: system design, implementation, and performance metrics. *IEEE Robot. Autom. Mag.* **31**, 25–37 (2024).
16. Yang, J. et al. Percutaneous nephrolithotomy guided by 5g-powered robot-assisted teleultrasound diagnosis system: first clinical experience with a novel tele-assistance approach (ideal stage 1). *BMC Urol.* **24**, 17 (2024).
17. Ferraguti, F. et al. Augmented reality and robotic-assistance for percutaneous nephrolithotomy. *IEEE Robot. Autom. Lett.* **5**, 4556–4563 (2020).
18. Taguchi, K. et al. The first case report of robot-assisted fluoroscopy-guided renal access during endoscopic combined intrarenal surgery. *J. Endourol. Case Rep.* **6**, 310–314 (2020).
19. Kok, E. N. et al. Accurate surgical navigation with real-time tumor tracking in cancer surgery. *NPJ Precis. Oncol.* **4**, 8 (2020).
20. de Baère, T., Roux, C., Deschamps, F., Tselikas, L. & Guiu, B. Evaluation of a new ct-guided robotic system for percutaneous needle insertion for thermal ablation of liver tumors: a prospective pilot study. *Cardiovasc. Interv. Radiol.* **45**, 1701–1709 (2022).
21. Grasso, R. F. et al. Lung thermal ablation: comparison between an augmented reality computed tomography (ct) 3d navigation system (sirio) and standard ct-guided technique. *Biology* **10**, 646 (2021).
22. Dirk Manski. Urology-Textbook.com, accessed 16 April 2025. https://www.urology-textbook.com/.
23. Siciliano, B., Sciavicco, L., Villani, L. & Oriolo, G. *Robotics: Modelling, Planning and Control* (Springer, 2010).
24. National Aeronautics and Space Administration. Official NASA Task Load Index, accessed 23 May 2024. https://humansystems.arc.nasa.gov/groups/tlx/.
25. Wilson, M. R. et al. Development and validation of a surgical workload measure: the Surgery Task Load Index (SURG-TLX). *World J. Surg.* **35**, 1961–1969 (2011).
26. Yu, D. et al. Quantifying intraoperative workloads across the surgical team roles: room for better balance? *World J. Surg.* **40**, 1565–1574 (2016).
27. Cevik, B. & Eryildirim, B. Anesthesia view in percutaneous nephrolithotomy: a 3-year experience of a referral hospital. *South. Clin. Istanb. Eurasia* **29**, 24–29 (2018).
28. Cekmen, N. Apneic oxygenation and anesthesia: mini review. *Int. J. Clin. Anesthesiol.* **11**, 1122 (2023).
29. Isensee, F., Jaeger, P. F., Kohl, S. A., Petersen, J. & Maier-Hein, K. H. nnu-net: a self-configuring method for deep learning-based biomedical image segmentation. *Nat. methods* **18**, 203–211 (2021).
30. Alex, D. M., Abraham Chandy, D., Hepzibah Christinal, A., Singh, A. & Pushkaran, M. Ysegnet: a novel deep learning network for kidney segmentation in 2d ultrasound images. *Neural Comput. Appl.* **34**, 22405–22416 (2022).
31. Hogan, N. Impedance control: an approach to manipulation. In *American Control Conference* 304–313 (IEEE, 1984).
32. Mathiassen, K., Dall'Alba, D., Muradore, R., Fiorini, P. & Elle, O. J. Robust real-time needle tracking in 2-d ultrasound images using statistical filtering. *IEEE Trans. Control Syst. Technol.* **25**, 966–978 (2017).
33. Müller, M. et al. Mobile augmented reality for computer-assisted percutaneous nephrolithotomy. *Int. J. Comput. Assist. Radiol. Surg.* **8**, 663–675 (2013).
34. Li, H. et al. Construction of a three-dimensional model of renal stones: comprehensive planning for percutaneous nephrolithotomy and assistance in surgery. *World J. Urol.* **31**, 1587–1592 (2013).
35. Vavra, P. et al. Recent development of augmented reality in surgery: a review. *J. Healthc. Eng.* **2017**, 4574172 (2017).

Acknowledgements

This work is part of the project "Robotic-assisted percutaneous nephrolithotomy with ultrasound guidance and 3D reconstruction superimposition", supported and funded by the European Union—NextGenerationEU.

Author contributions

F.F., S.B. and C.S. are robotics engineers. F.F. conceived the study design and wrote and reviewed the manuscript. S.B. implemented the system, conducted the technical part of the experiments, generated the figures and contributed to the video. He wrote and reviewed the manuscript. C.S. conceived the study design and reviewed the manuscript. S.P., G.B. and S.F. are urologists. S.P. and G.B. conceived the study design and provided the requirements and specifications. S.F. conducted participant recruitment and guided the residents during the experimental campaign. S.P., G.B. and S.F. executed the experiments and reviewed the manuscript.

Competing interests

Four authors of this manuscript (F.F., C.S., S.P., and G.B.) are inventors listed on a patent application filed in May 2024, which covers the conceptual idea described herein. The remaining authors declare no competing interests.

Additional information

Supplementary information The online version contains supplementary material available at https://doi.org/10.1038/s44172-025-00451-0.

Correspondence and requests for materials should be addressed to Stefano Bazzani.

Peer review information *Communications Engineering* thanks Junling Fu, Karen Stern, and the other, anonymous, reviewer for their contribution to the peer review of this work.